Mission Analysis and Systems Design of a Near-Term and Far-Term Pole-Sitter Mission

Jeannette Heiligers,[a*] Matteo Ceriotti,[a†] Colin R. McInnes[a‡] and James D. Biggs[a§]

[a]*Advanced Space Concepts Laboratory, Department of Mechanical and Aerospace Engineering, University of Strathclyde, 75 Montrose Street, Glasgow G1 1XJ, Scotland, United Kingdom.*

This paper provides a detailed mission analysis and systems design of a near-term and far-term pole-sitter mission. The pole-sitter concept was previously introduced as a solution to the poor temporal resolution of polar observations from highly inclined, low Earth orbits and the poor high-latitude coverage from geostationary orbit. It considers a spacecraft that is continuously above either the north or south pole and, as such, can provide real-time, continuous and hemispherical coverage of the polar regions. Being on a non-Keplerian orbit, a continuous thrust is required to maintain the pole-sitter position. For this, two different propulsion strategies are proposed, which result in a near-term pole-sitter mission using solar electric propulsion (SEP) and a far-term pole-sitter mission where the SEP thruster is hybridized with a solar sail. For both propulsion strategies, minimum propellant pole-sitter orbits are designed. In order to maximize the spacecraft mass at the start of the operations phase of the mission, the transfer from Earth to the pole-sitter orbit is designed and optimized assuming either a Soyuz or an Ariane 5 launch. The maximized mass upon injection into the pole-sitter orbit is subsequently used in a detailed mass budget analysis that will allow for a trade-off between mission lifetime and payload mass capacity. Also, candidate payloads for a range of applications are investigated. Finally, transfers between north and south pole-sitter orbits are considered to overcome the limitations in observations due to the tilt of the Earth's rotational axis that causes the poles to be alternately situated in darkness. It will be shown that in some cases these transfers allow for propellant savings, enabling a further extension of the pole-sitter mission.

Keywords: Pole-sitter, Polar observation, Trajectory optimization, Solar electric propulsion, Solar sailing, Hybrid propulsion

---

[*] Corresponding author. Tel.:+44 141 548 5989. E-mail address: Jeannette.Heiligers@strath.ac.uk

[†] Now at Systems Power and Energy division, School of Engineering, James Watt Building South, University of Glasgow, Glasgow G12 8QQ, Scotland, United Kingdom. Tel.: +44 141 330 6465. E-mail address: Matteo.Ceriotti@glasgow.ac.uk.

[‡] Tel.:+44 141 548 2049. E-mail address: Colin.McInnes@strath.ac.uk

[§] Tel.:+44 141 548 2042. E-mail address: James.Biggs@strath.ac.uk

1. Introduction

Spacecraft in geostationary orbit (GEO) have demonstrated the significant benefits offered by continuous coverage of a particular region. However, GEO platforms can only provide their services in the equatorial zone and at temperate latitudes (i.e. latitudes between the tropic and (ant)arctic circles), where elevation angles are sufficiently high. At higher latitudes, similar services are currently mainly provided by two types of conventional platforms: highly-eccentric, inclined orbits, or low or medium polar orbits.

The first class includes the well-known Molniya-type orbits. Due to their high ellipticity, their apocentre is usually at a distance that is comparable to GEO, and Molniya orbits therefore offer a hemispheric view of the Earth. However, the Molniya orbit has two intrinsic limitations. The first is the critical inclination of 63.4° or 116.6°, which does not allow for a satisfactory coverage of the polar caps or high-latitude regions [1]. Recent research [2] has therefore considered changing the critical inclination of the Molniya orbit to 90°, using a continuous solar electric propulsion (SEP) system for maintaining the orbit. However, a second limitation is the impossibility of providing continuous coverage over time. It was shown that from three up to six Molniya spacecraft are necessary to provide satisfactory continuous coverage [3].

The second class of orbits largely consists of Sun-synchronous orbits. Spacecraft in these orbits are used because of the high spatial resolution service that they can provide. However, only a narrow swath is imaged at each passage, relying on multiple passages (and/or multiple spacecraft) for full coverage. For example, Landsat 7 (altitude of 705 km at 98.2°) completes just over 14 orbits per day. Taking into account the field of view of Landsat 7, coverage of the entire Earth between 82.6 degrees north and south latitude is achieved every 16 days[**]. This results in a poor temporal resolution for the entire polar region, as different areas are imaged at different times. At present, these images are post-processed to make a composite image, which can be used, for example, for weather forecasting and wind vector prediction. However, the data that can be extracted is neither complete nor accurate [4].

To overcome these limitations, the ideal platform would be one with a continuous view of the poles for a long duration, or even better, one that is constantly above one of the poles, stationary with respect to the Earth, in the same way as a GEO spacecraft is stationary above one point on the equator. This spacecraft is known in the literature as "pole-sitter", which uses low-thrust propulsion to maintain a position along the Earth's rotational axis. As such, it is the only platform that can offer a truly continuous hemispheric view of one of the poles, enabling real-time imaging over the entire disc.

The first study of this concept was made by Driver [5] in 1980, although the author claims that the original idea belongs to the mathematician and writer Kurd Lasswitz from 1971. As investigated by Driver, in order to keep the pole-sitter spacecraft in a steady position on the Earth's rotational axis, a continuous acceleration has to be provided, to counterbalance mainly the gravitational attraction of the Earth and of the Sun. Driver proposed the use of SEP, which is now a mature technology, having flown on a number of missions (from NASA's Deep Space 1 in 1998 to ESA's GOCE in 2009): it provides the spacecraft with a relatively low thrust (in the order of a fraction of a New-

[**] Landsat 7 Handbook, http://landsathandbook.gsfc.nasa.gov/ [Cited 12/09/2011]

ton), but with a high specific impulse. However, the mission duration is always limited by the amount of propellant on-board.

In order to avoid this drawback, some authors investigated the use of a solar sail instead of SEP as a means to provide the continuous acceleration. Solar sailing [6] is a propellant-less spacecraft propulsion system that exploits the solar radiation pressure due to solar photons impinging on a large, highly reflecting surface (the sail) to generate thrust. Despite the original idea of solar sailing being rather old [7], only very recently has a spacecraft successfully deployed a solar sail: the IKAROS mission of the Japanese Aerospace Exploration Agency (JAXA) [8]. Due to the interesting potential of enabling missions that are not constrained by propellant mass, studies on potential solar sail missions have been undertaken, while others are still ongoing [9, 10]. These studies also include investigations for observing high-latitude regions. In particular, notable examples are those relying on artificial displaced equilibria and non-Keplerian orbits (NKOs) [11, 12]. A further comparison of these concepts is provided in Reference [1]. However, in all these mission concepts, the spacecraft does not achieve satisfactory conditions for continuous coverage of the high-latitude regions [1].

One of the intrinsic limitations of solar sailing is the relationship between the direction of the sail force vector and its magnitude; in particular, the force can never be directed towards the Sun, which is the reason why a sailcraft cannot maintain the pole-sitter position indefinitely [13]. In the effort of bypassing the limitations of SEP and solar sailing, a hybridization of these systems was proposed [14].

Hybrid solar sail and solar electric propulsion is a recent idea [14], nevertheless research is flourishing in this field, investigating its potential for novel, interesting applications: artificial equilibria above L_1 in the Sun-Earth system for Earth observation [15], optimal interplanetary transfers to Venus and Mars [16], displaced periodic orbits in the Earth-Moon system [17] and displaced NKOs for geostationary coverage [18]. The reason for this interest is due to the fact that in the hybrid system, at the cost of increased spacecraft and mission design complexity, the two propulsion systems complement each other, cancelling their reciprocal disadvantages and limitations. [13]

Although the hybrid propulsion pole-sitter can in principle enable a mission that is not feasible using only a solar sail and can extend the mission lifetime with respect to the pure SEP scenario, still an issue exists in relation to the pole-sitter, namely its large distance from the Earth. It was in fact shown that the acceleration required increases dramatically when the spacecraft gets closer to the Earth, and reasonable values of acceleration are obtained only if the spacecraft is in the range of millions of kilometers from the Earth [5, 13]. This means that these types of platforms will certainly not be used in the near future for high-bandwidth telecommunications and high-resolution imagery. However, a number of novel potential applications can be enabled, both in the fields of observation and telecommunications. A complete discussion of possible applications is presented in Reference [1] and include continuous views of dynamic phenomena and large-scale polar weather systems [19], polar ice shield and sea-ice monitoring [4], space weather monitoring [19], data relay with polar regions [4] and ship tracking and telecommunications especially if the northern sea routes open up due to global warming.[††]

[††] http://www.esa.int/esaEO/SEMT7TRTJRG_index_0.html [cited 12/09/2011].

Due to the potential number of applications, the authors have undertaken an extensive investigation, focused on the study of the concept of a hybrid-propulsion pole-sitter, with the aim of increasing the potential mission lifetime. Recent publications studied and covered different parts of the mission, from the generation of optimal hybrid pole-sitter orbits [13] to a systems mass budget [20] and from the design of optimal transfers to the pole-sitter from LEO [21] to the design of optimal north-to-south transfers [22]. However, a complete end-to-end mission design, including the trajectory and the spacecraft sizing, has never been presented.

This paper therefore presents the full mission analysis and systems design of a pole-sitter mission. Several different options will be proposed and assessed, including different propulsion systems for the spacecraft (SEP or hybrid sail-SEP), different launch options and different operations phases, enabling coverage of one pole only or both poles. For that, the authors partially exploit the techniques that were developed previously in order to provide a preliminary analysis of an entire pole-sitter mission.

2. Dynamics, Architectures and Mission Scenarios

2.1 Equations of motion

For the transfer and operations phases, we consider a three-body problem in which the spacecraft is subject to the gravitational attraction of both the Earth and the Sun. This choice is made since the gravity of both the Earth and the Sun play an important role for the pole-sitter. In particular, we use the well-known circular restricted three-body problem (CR3BP), which describes the motion of the spacecraft, of negligible mass, under the influence of the Sun and Earth (the primaries) that are assumed to rotate in circular motion around each other. The reference frame is synodic, with its origin at the center of mass of the system, the x-axis passing through the Sun and the Earth, and oriented towards the latter, and the z-axis aligned with the angular velocity vector of the primaries, see Figure 1. The equations of motion for a spacecraft at position **r** in this frame can be written as [23]:

$$\ddot{\mathbf{r}} + 2\boldsymbol{\omega}\times\dot{\mathbf{r}} + \boldsymbol{\omega}\times\left(\boldsymbol{\omega}\times\mathbf{r}\right) - \nabla\left(\frac{Gm_S}{r_1} + \frac{Gm_E}{r_2}\right) = \mathbf{a}$$

where $\boldsymbol{\omega} = 2\pi/\text{year}\,\hat{\mathbf{z}}$ is the angular velocity vector of the primaries, $\mathbf{a}$ is the total acceleration provided by the spacecraft propulsion system, $Gm_E = 4.0351\cdot10^5$ km^{3}s^{-2} is the gravity constant of the Earth-Moon system, and $Gm_S = 1.3272\cdot10^{11}$ km^{3}s^{-2} that of the Sun. The vector differential equation can be re-written as a set of first-order scalar differential equations by introducing the state vector $\mathbf{x} = \begin{bmatrix}\mathbf{r}^T & \mathbf{v}^T & m\end{bmatrix}^T$, including an additional equation for the mass *m* of the spacecraft:

$$\dot{\mathbf{x}} = \begin{bmatrix}\dot{\mathbf{r}}\\ \dot{\mathbf{v}}\\ \dot{m}\end{bmatrix} = \begin{bmatrix}\mathbf{v}\\ -2\boldsymbol{\omega}\times\dot{\mathbf{r}} - \boldsymbol{\omega}\times\left(\boldsymbol{\omega}\times\mathbf{r}\right) + \nabla\left(\frac{Gm_S}{r_1} + \frac{Gm_E}{r_2}\right) + \mathbf{a}_s + \mathbf{a}_T\\ -m\mathbf{a}_T/I_{sp}g_0\end{bmatrix} \qquad (1)$$

where the total acceleration is now split into the two components, $\mathbf{a}_s$ and $\mathbf{a}_T$, due to the sail and the SEP system, respectively. The mass flow depends only on the part of acceleration provided by the SEP system, $\mathbf{a}_T$, through the SEP thruster specific impulse, I_{sp}, and $g_0 = 9.81\ \mathrm{m/s^2}$.

Note that, for the first part of the transfer from Earth to the pole-sitter orbit, a Keplerian two-body approach will be considered, rather than the three-body approach presented here, since the spacecraft is relatively close to the Earth during that part of the transfer. More details on this can be found in Section 5 that describes the launch and transfer phase.

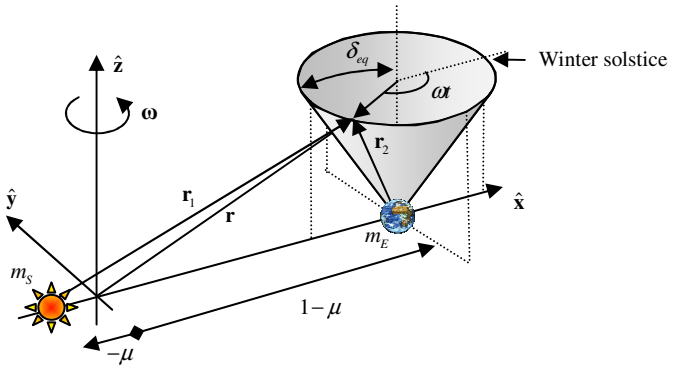

Figure 1. Restricted three-body problem and pole-sitter reference.

2.2 Spacecraft architectures

We consider two different spacecraft architectures. The first is a pure SEP spacecraft, in which solar electric propulsion is used to provide the acceleration needed throughout the mission. Due to the high TRL of this type of propulsion, the mission can be considered to be near-term. The second is a more advanced, far-term spacecraft that exploits both solar sail and solar electric propulsion on the same bus.

Pure SEP

The pure SEP spacecraft can be imagined as a conventional spacecraft with deployable solar panels to power the propulsion system. Usually, the solar panels can be rotated along their axis, such as to modulate the collected power according to the instantaneous need of the spacecraft. The thruster is rigidly connected to the spacecraft bus, and the thrust vector is steered by changing the attitude of the spacecraft (the instruments can be mounted on a gimbal).

The key technology parameters of an SEP thruster are the maximum thrust that it can provide, usually in the order of a fraction of a Newton, and its specific impulse. In this paper, we assume that the maximum thrust is used to size the SEP system, as will be explained later, and a fixed specific impulse of $I_{sp} = 3200\ \mathrm{s}$ is conservatively assumed, based on current ion engine technology (existing NSTAR/DS1 [24] or EADS/Astrium RIT-XT [25]). It is foreseen that this impulse allows levels of thrust suitable for the spacecraft and mission under consideration. Higher values of specific impulse can be achieved with current SEP technology, for example FEEP thrusters can provide up to 10,000 s, but the thrust is limited to very small values of 2 mN [26].

For a pure SEP spacecraft, the generated acceleration is simply given through:

$$\mathbf{a}_T = \mathbf{T}/m \tag{2}$$

and $\mathbf{a}_s = 0$. Therefore, the controls are the three components of the thrust vector $\mathbf{T}$.

Since the fuel mass consumption is strictly related to the magnitude of the thrust, in general we will try to find trajectories that minimize propellant consumption, in order to maximize the mission lifetime, or alternatively to maximize the payload mass for a given lifetime.

Hybrid Sail and SEP

In this scenario, we envisage the use of a spacecraft that combines solar sailing and SEP. As mentioned, this adds system complexity, but it can be advantageous in terms of mission lifetime, as will be shown in this paper.

The hybrid spacecraft is made of a bus from which the sail is deployed, and thus the sail is rigidly connected to it. We assume that the sail can be steered, with relatively modest angular acceleration, by using the attitude control system of the spacecraft. The SEP thruster is also mounted on the spacecraft bus; however, for control purposes, it is required that the SEP thrust vector can steer independently of the sail orientation throughout the mission. Therefore, the thruster shall be mounted on a gimbal system. Furthermore, the SEP system requires electrical power in order to operate. In conventional spacecraft, this is collected through solar panels that are hinged on the spacecraft bus and can be oriented towards the Sun when power is needed. This type of architecture would be difficult to implement due to the presence of the sail. We instead envisage a layer of thin film solar cells (TFSC) which partly occupy the sail surface, similarly to the IKAROS spacecraft [27].

As indicated previously, the total propulsive acceleration $\mathbf{a}$ in Eq. (1) can be split into two components, $\mathbf{a}_T + \mathbf{a}_s$. The first is the SEP acceleration, which is given in Eq. (2), while the second is the acceleration provided by the sail. Assuming a partially absorbing solar sail of total area *A*, the latter can be expressed as [6]:

$$\mathbf{a}_s = \frac{1}{2}\beta_0 \frac{m_0}{m}\frac{Gm_S}{r_1^2}\left[g\cos\alpha\hat{\mathbf{n}} + h\sin\alpha\hat{\mathbf{t}}\right]\cos\alpha \tag{3}$$

Here $\hat{\mathbf{n}}$ is the component normal to the sail and $\hat{\mathbf{t}}$ parallel to it, in the plane of the Sun vector and normal vector (see Figure 2). m_0 and m are the spacecraft mass at a reference point of the mission and at any given time, respectively. In this paper, the reference point is the injection into the pole-sitter operations orbit, and the subscript "0" will be used to refer to variables at this point, when time is t_0.

β is the *system lightness number*, which is a function of the sail loading $\sigma = m/A$ of the spacecraft (spacecraft mass over sail area):

$$\beta = \sigma^*/\sigma$$

which can also be defined as the ratio of solar radiation pressure acceleration to the gravitational acceleration. The parameter $\sigma^* \cong 1.53\cdot 10^{-6}$ g/m^2 is the critical sail loading. Values of β up to 0.05 can be assumed for a near-term hybrid system [28]. Recent solar sail demonstrators, however, had considerably lower lightness numbers: JAXA's IKAROS [29] has a 20-m-diagonal square sail and weighs 350 kg (β = 0.001), while NASA's NanoSail-D2 [30] is 4 kg for 10 m^2 (β = 0.003). In the hybrid case, the spacecraft mass varies due to the SEP propellant consumption,

and so does the acceleration from the sail and the value β; the value β_0, however, remains constant. Finally, the pure SEP spacecraft can be considered as a particular hybrid system with $\beta = 0$.

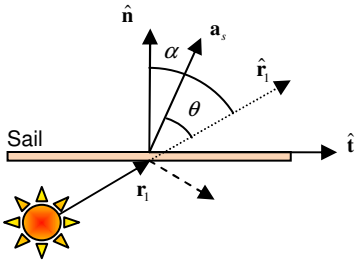

Figure 2. Optical sail angles.

The direction of the sail acceleration $\hat{\mathbf{a}}_s$ is related to the sail normal $\hat{\mathbf{n}}$ through the coefficients *g* and *h* [15], which can be computed as a function of the reflectivity of the sail, $\tilde{r}_s = 0.9$, and of the thin film, $\tilde{r}_{TF} = 0.4$ [14]:

$$g = 1 + \tilde{r}_s + \frac{A_{TF}}{A}\left(\tilde{r}_{TF} - \tilde{r}_s\right); \qquad h = 1 - \tilde{r}_s - \frac{A_{TF}}{A}\left(\tilde{r}_{TF} - \tilde{r}_s\right)$$

Non-specular reflection and emission are not considered in the solar sail model. In the hybrid spacecraft, the TFSCs cover an area $A_{TF} = 0.05A$ of the sail. This area ratio is a conservative estimation based on previous studies [15] and the IKAROS mission [29], and it is used to compute the optimal pole-sitter orbits. The actual value of this area depends on the spacecraft technology parameters, as well as the selected orbit, and it will be computed in a later section.

The cone angle of the sail $\alpha \in [0, 90°]$ measures the angle between the sail normal and the Sun direction. When the sail is perpendicular to the Sun vector ($\alpha = 90°$) at 1 Astronomical Unit (AU, 149.6 million km), the acceleration produced by the sail is known as the characteristic acceleration (a_c). Any of the three parameters β, σ and a_c are indicators of the technology needed for the spacecraft: the larger the lightness number is, the lower the sail loading is. This is achieved either using a larger sail area, or by reducing the system or sail mass.

Another important technological parameter of a sailcraft is the areal density of the sail assembly σ_s. It measures the mass of the sail per unit surface area, and it is expected that technological developments [28] should enable sails of 10 g/m^2 in the near future. Ultra-thin (around 2 μm of thickness) sails are expected in the mid- to far-term timeframe [31] and can lead, for large sails, to sail loadings of the order of 5 g/m^2.

The value of β_0 for the hybrid scenario can be decided following the study in Reference [20]. That work showed that, if a sail assembly areal density of 10 g/m^2 is considered, then the hybrid spacecraft is beneficial only if very long missions are considered (i.e. lifetime > 7 years). Instead, considerable mass saving (or extended lifetime) is expected considering a hybrid system with $\sigma_s = 5$ g/m^2 (or less). Furthermore, for this value, it results that $\beta_0 = 0.035$ represents the lightness number in which the spacecraft initial mass, for a given payload, is lowest over a range of mission lifetimes. For these reasons, we select for this scenario: $\beta_0 = 0.035$, $\sigma_s = 5$ g/m^2.

Finally, the controls of the hybrid spacecraft are the SEP thrust vector $\mathbf{T}$ (three components), and additionally the sail attitude $\hat{\mathbf{n}}$ (two angular components), which through Eq. (3) defines the sail acceleration $\mathbf{a}_s$.

3. Mission phases

The pole-sitter mission is split into different phases, which will be described in detail and designed in the following sections. The phases are schematically represented in Figure 3.

The mission starts with a launch and transfer phase. This phase starts with the spacecraft injected into a low Earth orbit (LEO) by the launcher, of which the type and size depend on the launcher used. An optimization process subsequently finds a number of impulsive maneuvers to be performed by the launcher upper-stage. The upper-stage is then jettisoned and the spacecraft continues the transfer using its own low-thrust propulsion system, up to the injection point into the pole-sitter orbit.

At this point, the operations phase begins. The operations phase is the one in which the spacecraft is aligned with the rotational axis of the Earth, and therefore the spacecraft is fully operative. This is obviously the most important phase of the mission, and the time in which the spacecraft maintains this position shall be maximized to maximize the scientific return.

Since each pole is lit only 6 months per year, it is an option, especially for observations in the visible part of the spectrum, to transfer the spacecraft from a north pole operations orbit to a symmetric orbit below the south pole, and vice-versa, according to their lighting conditions. Therefore, an additional north-to-south transfer phase is designed. This phase can be inserted at appropriate points along the nominal orbit to enable the transfer to the other pole, where a symmetric operations orbit can be followed.

These three phases will be described and designed sequentially, starting from the operations phase, which defines the optimal nominal orbit. Then, the transfer from Earth to this orbit will be designed. The optimization of the transfer allows the determination of the maximum mass at the pole-sitter orbit injection, and therefore the spacecraft can be sized and the lifetime assessed. Finally, the north-to-south transfers between the optimal pole-sitter orbits will be designed.

The design of the three phases requires the solution of optimal control problems, which are solved numerically using a direct method based on pseudospectral transcription, implemented in the tool PSOPT. PSOPT is coded in C++ by Becerra [32] and is free and open source. PSOPT can deal with endpoint constraints, path constraints, and interior point constraints. Bounds on the states and controls can be enforced, as well as intervals for initial and final states [33]. It makes use of the ADOL-C library for the automatic differentiation of objective, dynamics and constraint functions. The NLP problem is solved through IPOPT [34], an open source C++ implementation of an interior point method for large scale problems.

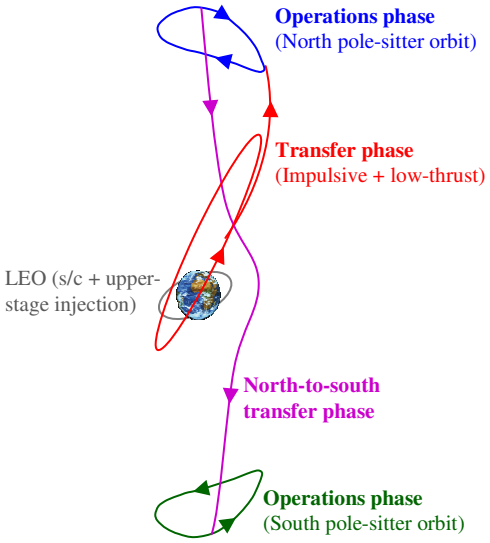

Figure 3. Representation of the mission phases.

4. Pole-Sitter Operations Orbits

In this section, we design an optimal pole-sitter orbit for each of the two types of spacecraft under consideration.

A pole-sitter spacecraft is constantly aligned with the rotational axis of the Earth. We can consider that the direction of the rotational axis of the Earth is inertially fixed while the Earth is orbiting the Sun (in other words, we are neglecting the nutation of the Earth's rotational axis and the precession of the equinoxes). In the synodic ecliptic reference frame, the same axis rotates with a motion of apparent precession, due to the obliquity of the ecliptic: its angular velocity is $-\boldsymbol{\omega}$ (see Figure 1). Therefore, the Earth's rotational axis spans a full conical surface every year, in a clockwise direction (refer again to Figure 1). The cone half angle is the tilt of the axis relative to the ecliptic, i.e. $\delta_{eq} = 23.5$ deg . The position of the spacecraft is to be constrained to follow this clockwise apparent precession of the Earth's rotational axis, and hence maintain the pole-sitter condition. Without loss of generality, we consider the time $t_0 = 0$ as the winter solstice, and therefore the spacecraft's position is constrained to be:

$$\mathbf{r}(t) = \begin{bmatrix} r_2(t)\sin\delta_{eq}\cos\omega t + (1-\mu) \\ -r_2(t)\sin\delta_{eq}\sin\omega t \\ r_2(t)\cos\delta_{eq} \end{bmatrix} \tag{4}$$

with μ the barycenter-Sun distance, see Figure 1. $r_2(t)$ is the only free variable, is a function of time and represents the distance of the spacecraft from the Earth. Equation (4) refers to a north pole orbit, and the south pole case can be obtained by simple symmetry considerations. Once again, Figure 1 represents a particular pole-sitter orbit in which $r_2(t)$ is constant. In that particular case, where the Earth-spacecraft distance remains unchanged, the propulsive acceleration required to maintain the pole-sitter position can easily be computed by considering a reference frame centered at the Earth and summing the gravitational forces of the Earth and the Sun, which need to be

counterbalanced by the propulsion system. However, in this paper, an optimal pole-sitter orbit is sought for, which is defined as the one that minimizes the propellant consumption of the spacecraft, while maintaining the pole-sitter condition at any time (i.e. satisfy Eq. (4)), and being one-year periodic. The design of this orbit requires the (numerical) solution of a constrained optimal control problem, in which the control and state history over time is to be determined.

The implicit approximation that is made here is that the optimal control problem is solved only for the first year (or period) of the mission, and the same trajectory is then used for following years. In reality, a fully optimized trajectory would change year by year, due to the change in mass of the spacecraft. In other words, the optimal control problem should be solved not only for one year, but for the entire mission lifetime at once. However, the lifetime cannot be determined at this stage, and the full optimization would result in very minor differences in the results, and therefore it is not considered in this paper.

As can be seen from the equations of motion in Eq. (1), the mass of the spacecraft is one component of the spacecraft state vector. However, at this stage, the (initial) mass is not known as it depends on the launcher performances and the transfer phase; however, both of them in turn depend on the optimal pole-sitter orbit that is selected. However, if the SEP system can provide the acceleration required by the optimal trajectory at any time (i.e. the constraint on the maximum thrust is not active), then the problem is fully scalable on the initial mass, and it can be solved for an arbitrary initial mass.

In the optimization process, the maximum distance from the Earth is limited to $d_{max} = 0.01831$ AU, i.e. about 2.74 million km, in order to prevent the trajectory from going too far away from the Earth, thereby excessively decreasing the spatial optical resolution or the data bandwidth of the platform. In fact, it was found [13] that optimal, unconstrained trajectories are those that go further away from the Earth in summer, which is the period in which the north pole is lit, and therefore observations in the optical wavelength can be performed.

Details of the optimization process are presented in Reference [13]. As noted, the optimal control problem is solved with PSOPT, and the first guess is found through an inverse approach, in which a trajectory satisfying the constraints is assumed (although non-optimal) and the controls for this trajectory are derived through a semi-analytical procedure.

The result of the optimization, for the two scenarios, is presented in the following figures. The orbital graphs are presented in an Earth centered (rather than barycentric) synodic reference frame for easy interpretation. The optimal SEP-only path is essentially symmetric around spring and autumn, and the spacecraft is closest to the Earth at the summer and winter solstices. Instead, in the hybrid case, the spacecraft is closest to the Earth in winter and farthest in summer: the constraint on the maximum distance is active across the summer solstice for about 150 days. This is visible in Figure 4. The same figure also highlights that the SEP spacecraft distance to the Earth varies between 0.01568 and 0.01831 AU, while for the hybrid case it varies between 0.01369 and 0.01831 AU.

Figure 5 instead plots the modulus of the SEP acceleration as function of time in the two scenarios, which shows that the hybrid case needs less acceleration due to the contribution of the sail.

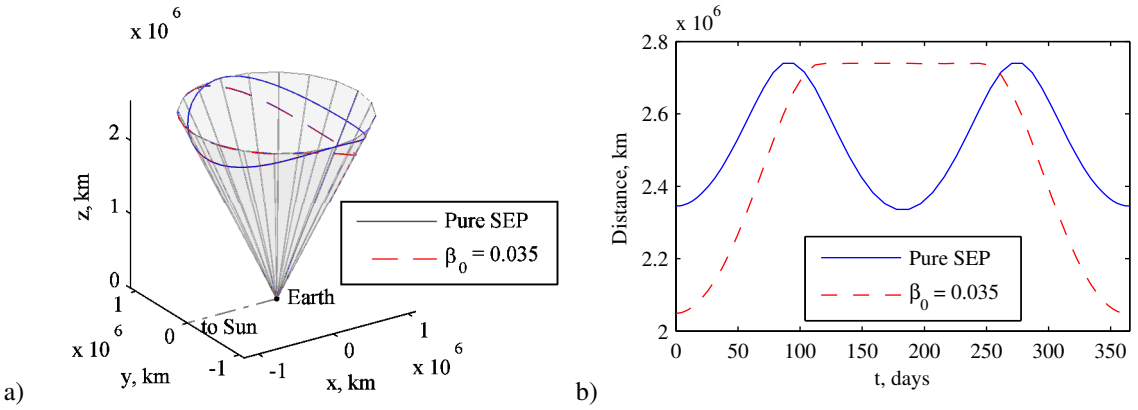

Figure 4. Fuel-optimal pole-sitter orbits for the pure SEP case and the hybrid case. (a) Optimal trajectories in the synodic reference frame. (b) Distance from the Earth.

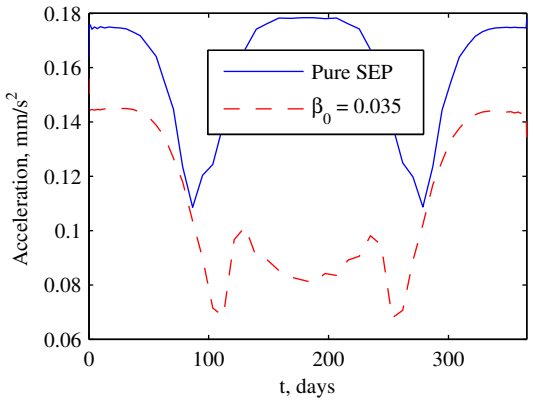

Figure 5. SEP acceleration (modulus) required for the pure SEP case and the hybrid case.

Since we stated that the problem is scalable with the initial mass, then we can say that the maximum thrust needed can be found through a multiplication with the SEP acceleration in Figure 5, once the mass at injection is known. Due to the periodicity of the orbit, the maximum thrust is achieved in the first period, when the spacecraft mass is highest; observing the acceleration over one period in Figure 5, we can also infer that the maximum thrust is required at winter solstice, which coincides with pole-sitter injection as will be shown in the next section.

This value of the maximum thrust is the one that the SEP system shall provide for maintaining the orbit, and is also used to size the propulsion subsystem itself. For example, for a spacecraft of 1000 kg at injection, the maximum SEP thrust would be 170 mN for the pure SEP system, and 144 mN for the hybrid system.

5. Launch and Transfer phase

As stated before, we wish to find optimum transfers from LEO up to injection into the pole-sitter orbit such that the mass upon injection is maximized and the maximum mission lifetime or payload capacity can be obtained. To find these optimal transfers, the transfer is modeled by distinguishing between a launch phase and a transfer phase, as shown in Figure 3. The launch phase is designed as an impulsive, two-body Soyuz or Ariane 5 upper-stage transfer

from a fixed inclination low Earth parking orbit up to insertion into the transfer phase. This second, low-thrust transfer phase is subsequently modeled in the Earth-Sun three body problem using Eq. (1). Furthermore, either pure SEP or hybrid propulsion is used in the transfer, depending on the system architecture. PSOPT solves the optimal control problem in the transfer phase and patches the launch phase to the transfer phase in an end-point constraint. More details on this approach as well as the generation of suitable initial guesses can be found in Reference [21]. However, the optimization in Reference [21] considers a fixed mass upon injection into the pole-sitter orbit (i.e. 1000 kg) and minimizes the mass required in LEO, while the approach considered in this paper fixes the mass in LEO (i.e. maximum launcher performance) and maximizes the mass upon insertion. Hereafter some details on the Soyuz and Ariane 5 launch phases will be given, followed by the results obtained.

5.1 Soyuz launch vehicle

In previous work, a launch model was developed that was shown to accurately match the Soyuz launch vehicle performance provided by the Soyuz manual in Reference [35]. The model assumes that the first three stages of the Soyuz are launched from Baikonur and are used to reach a LEO with an altitude of 200 km and with one of four reference inclinations: 51.8, 64.9, 70.4 and 95.4 deg. Depending on the inclination, the Soyuz launch vehicle can provide payload masses of 6275 kg (95.4 deg) to 7185 kg (51.8 deg) to this parking orbit. From the parking orbit, any remaining inclination and altitude changes can be provided by the Fregat upper-stage through a two-body Hohmann-type transfer to the final target orbit. This final target orbit then coincides with the start of the low-thrust transfer phase. Simple and well-known Hohmann transfer formulas [36] and the rocket equation are subsequently used to provide the mass that can be delivered to the final target orbit. A validation of this launch model is given in Reference [21]. It is important to highlight this model can only consider non-escape launches, meaning that the eccentricity at the end of the launch phase, and thus at the start of the transfer phase, should be less than 1.

Clearly, any of the four parking orbit inclinations could be used for the pole-sitter transfer. However, because the pole-sitter can be viewed as having an inclination of 90 degrees, one could expect that, the closer the inclination of the parking orbit is to the inclination of the pole-sitter, the better the performance in terms of mass at pole-sitter injection. On the other hand, the smaller the parking orbit inclination, the better the Soyuz performance in the parking orbit (a difference of over 900 kg exists between the performances in the 51.8 and 95.4 deg parking orbits). Initial results have indeed shown that this higher mass in the parking orbit eventually translates into a larger mass at injection than when considering a parking orbit with an inclination closer to the inclination of the pole-sitter orbit. Therefore, the remaining analyses in this section will assume a parking orbit inclination of 51.8 degrees. An overview of the final parking orbit parameters and details of the Soyuz Fregat upper-stage are given in Table 1.

Table 1. Soyuz and Ariane 5 parking orbit and launch vehicle specifications.

Launcher	Parking orbit			Upper stage		Adapter
	Altitude, km	Inclination, deg	Performance,[‡‡] kg	Mass, kg	Specific impulse, s	Mass, kg
Soyuz	200	51.8	7185	1000	330	100
Ariane 5	400	51.6	19000	4540	446	160

5.2 Ariane 5 launch vehicle

For comparison purposes, and also because less detailed information is available in the literature for the performance of the Ariane 5 launch vehicle, it is assumed that a similar launch strategy can be adopted for the cryogenic upper-stage (ESC-A) of the Ariane 5. However, the parking orbit is assumed to be equal to the orbit of the International Space Station (400 km altitude and 51.6 deg inclination), for which it is given that Ariane 5 can deliver 19 t [37]. Other details of the Ariane 5 upper-stage are provided in Table 1.

5.3 Results

Starting with the pure SEP case, the results are provided by the dotted lines in Figure 6. The figure shows that the optimal transfer injects the spacecraft at winter solstice, i.e. at the point closest to the Earth. Due to the symmetry of the pole-sitter orbit a similar, equally optimal trajectory can be found at summer solstice.

More details on the optimal SEP transfer, including the maximum thrust magnitude and mass injected into the pole-sitter orbit can be found in Table 2. The value for the maximum thrust magnitude is obtained through an iterative approach, where an initial value is assumed, which is updated by multiplying the corresponding optimized injected mass with the maximum acceleration in the pole-sitter orbit as discussed at the end of the previous section.

Comparing the performances of the Soyuz and Ariane 5 launch vehicles shows an increase in the mass injected into the pole-sitter orbit by a factor 2.9 for an Ariane 5 launch: 1535 kg versus 4432 kg. A similar increase can be observed for the maximum thrust magnitude. Because the maximum thrust magnitude is allowed to scale with the increase in the injected mass that the Ariane 5 launch can establish, the results in Figure 6 show a very clear scalability of the transfer. Any differences between the two transfers can be attributed to the slightly different parking orbits from which the transfer is initiated.

Using the results for the SEP case as an initial guess for the hybrid transfer, the other results in Figure 6 and Table 2 can be found. Since the SEP and hybrid pole-sitter orbits are not the same, a direct comparison of the performances of the transfers using the two propulsion techniques cannot be made. However, the mass injected into the hybrid pole-sitter orbit is larger than for the SEP case: an increase of 58 kg for a Soyuz launch and an additional 160 kg for an Ariane 5 launch. Part of this better performance will be due to the smaller Earth to pole-sitter distance at winter solstice (i.e. upon injection) for the hybrid pole-sitter orbit. However, part will also be due to the smaller propellant

[‡‡] Including upper-stage and adapter mass.

consumption in the transfer. This becomes clear from comparing the thrust profiles in Figure 6 as the hybrid case allows for a much longer time in which the SEP thruster is switched off due to the contribution of the solar sail.

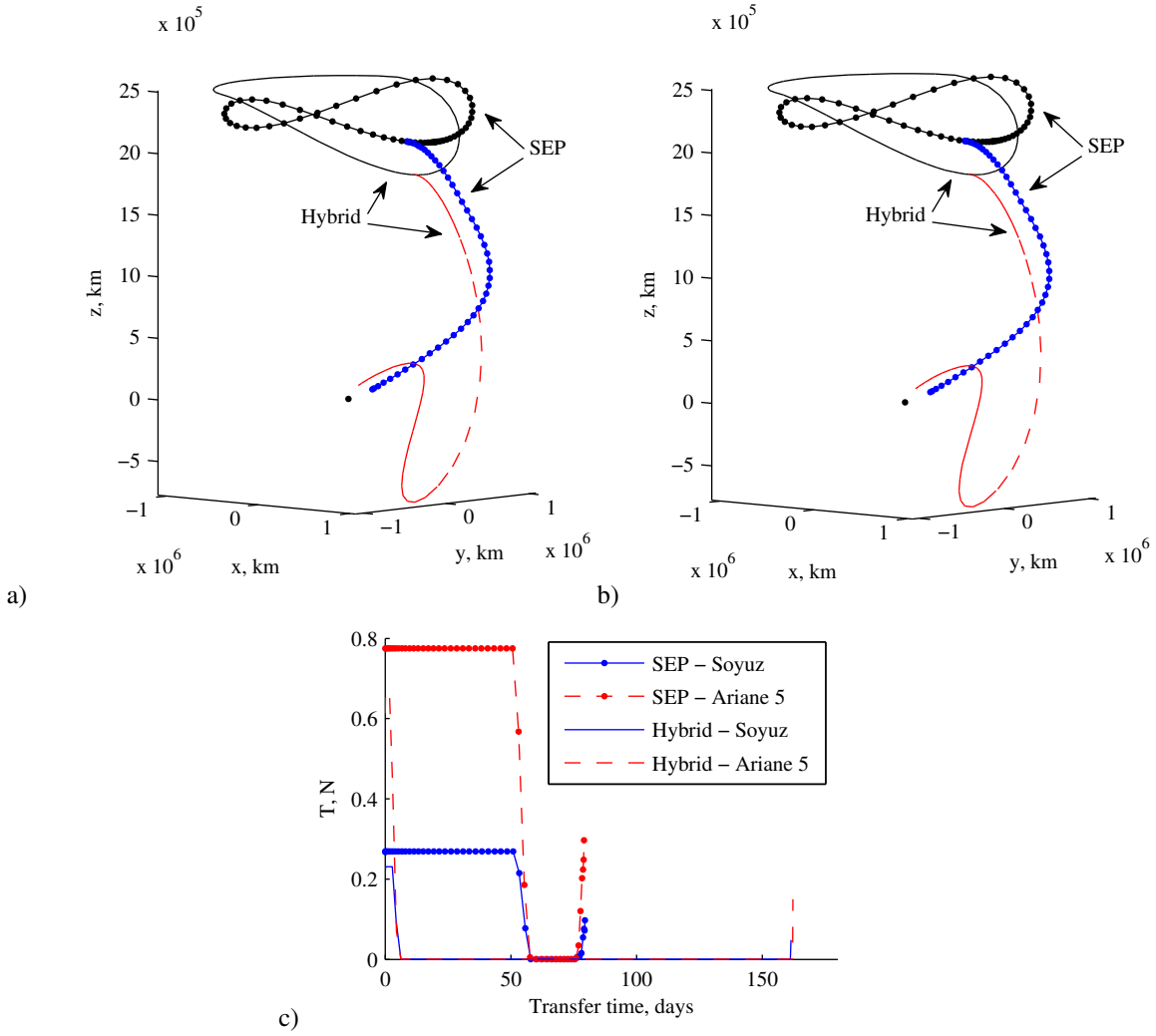

Figure 6. Optimal transfers to SEP and hybrid pole-sitter orbits for a Soyuz and Ariane 5 launch. Soyuz (a) and Ariane 5 (b) transfer in synodic reference frame. c) Thrust profile.

Table 2. Results for the optimization of the transfer to SEP and hybrid pole-sitter orbits including the maximum SEP thrust magnitude and the mass injected into the pole-sitter orbits.

Architecture	Launcher	T_{max} , N	m_0 , kg
SEP	Soyuz	0.269	1537
SEP	Ariane 5	0.775	4439
Hybrid	Soyuz	0.231	1595
Hybrid	Ariane 5	0.667	4599

6. Spacecraft and Payload sizing

Now that the mass that can be injected into the operations orbit of the pole-sitter is known, a systems design provides the mission lifetime that can be achieved in this orbit, or alternatively the payload mass that can be carried for a given lifetime of the spacecraft. This estimation is the subject of this section.

For a preliminary mass budget, the total mass of the pure SEP spacecraft can be split as:

$$m_0 = \left[m_{prop} + m_{tank} + n_{thrusters} m_{thruster} + m_{SA} + m_{other} \right] \left(1 + \varepsilon_{old}\right) + m_{pl} \tag{5}$$

and for the hybrid propulsion spacecraft:

$$\begin{aligned} m_0 = &\left[m_{prop} + m_{tank} + n_{thrusters} \left(m_{thruster} + m_{gimbal} \right) + m_{rad} + m_{other} \right] \left(1 + \varepsilon_{old}\right) + \\ &+ \left[m_s + m_{TF} \right] \left(1 + \varepsilon_{new}\right) + m_{pl} \end{aligned} \tag{6}$$

The subscripts '*prop*', '*SA*', '*pl*', '*rad*', '*s*' and '*TF*' refer to propellant, solar arrays, payload, radiator, solar sail and thin film solar cells, respectively, while the subscripts 'old' and 'new' for the margin ε refer to existing and new technologies. Further details of some of the mass components will be provided below and Table 3 summarizes the formulas used for each subsystem and for each configuration, highlighting the differences between the pure SEP and the hybrid spacecraft. In addition, some detailed considerations for some of the components are provided hereafter.

In the hybrid spacecraft, the sail, fixed to the spacecraft bus, determines the attitude of the bus itself. Therefore, a gimbal system is required to point the thrust vector independently from the spacecraft (within limits due to the system configuration); instead, for the pure SEP spacecraft, no gimbal is used, as the attitude of the three-axis stabilized spacecraft can be changed to orientate the thrust vector in the required direction. It is important to highlight that the mass of the total SEP subsystem does not depend on the number of thrusters, as it is assumed that all of them contribute equally to the thrust.

The mass of the solar array needed to generate power for the SEP thruster is proportional to its area. The area of the solar array A_{SA} can be estimated as a function of the maximum power. For the pure SEP spacecraft, the solar panels are usually kept perpendicular to the Sun vector. In the hybrid spacecraft, instead, the TFSC is part of the reflective surface, and therefore its pitch with respect to the Sun vector is given by the cone angle of the sail $\alpha = \alpha_{T_{max}}$ at the instant when the maximum thrust is required.

Radiators are employed to dissipate the excess power produced by the TFSC on the hybrid spacecraft (whose attitude with respect to the Sun is constrained by the sail attitude). Radiators are sized considering the minimum SEP thrust throughout the mission, and calculating the excess of power $P_{d,max}$ generated by the panels at that instant of time, and so the power that is to be dissipated.

The total sail area (highly reflective surface + TFSC) can be computed starting from the assumed values for β_0 and the optimized value for m_0. The area of the reflective part is simply $A_s = A - A_{TF}$, and its mass is $m_s = \sigma_s A_s$, where σ_s is the mass per unit area of the sail, as discussed in Section 2.2.

Finally, the mass of the other subsystems (ADCS, thermal, structure, OBDH, TT&C) is estimated as a fraction of the spacecraft dry mass $m_{dry} = m_0 - m_{prop}$.

Margins are taken into account for each subsystem [38]. In particular, the sail and the thin film solar cells are considered new technologies, and therefore a margin of $\varepsilon_{new} = 0.20$ is used. Conversely, the other subsystems are considered to be well-proven technologies, and their margin is set to $\varepsilon_{old} = 0.05$. The same margin is added to the propellant mass for contingency maneuvers.

Table 3. Subsystem mass budget for the pure SEP and the hybrid spacecraft.

	Pure SEP	Hybrid
Tank mass	$m_{tank} = 0.1 m_{prop}$	
Maximum SEP power [39]	$P_{SEP,max} = T_{max} I_{sp} g_0 / 2\eta_{SEP}$ $\eta_{SEP} = 0.7$	
SEP thruster (each) [24]	$m_{thruster} = k_{SEP} P_{SEP,max} / n_{thrusters}$ $k_{SEP} = 20\,\mathrm{kg/kW}$	
SEP thruster gimbal [40]	N/A	$m_{gimbal} = 0.3 m_{thruster}$
Solar arrays (thin film solar cells or solar panels) [14, 38] $W = 1367\ \mathrm{W/m^2}$	$A_{SA} = P_{SEP,max} / W\eta_{SA}$ $\eta_{SA} = 0.10$ $m_{SA} = \sigma_{SA} A_{SA}$ $\sigma_{SA} = 5.468\ \mathrm{kg/m^2}$	$A_{TF} = P_{SEP,max} / W\eta_{TF} \cos\alpha_{T_{max}}$ $\eta_{TF} = 0.05$ $m_{TF} = \sigma_{TF} A_{TF}$ $\sigma_{TF} = 100\ \mathrm{g/m^2}$
Solar sail	N/A	$m_s = \sigma_s A_s$
Radiators [38]	N/A	$m_{rad} = 0.0086\ \mathrm{kg/W} \cdot P_{d,max}$
Dry mass	$m_{dry} = m_0 - m_{prop}$	
Other subsystems [38]	$m_{other} = 0.3 m_{dry}$	

The systems mass budget proposed here differs to the one in Reference [20] in several ways: it considers multiple SEP thrusters, but working in parallel to achieve the necessary thrust, rather than being redundant; the mass of the other subsystems is now taken into account, and not considered as "payload" mass; the pure SEP spacecraft does not employ thin film solar cells, but solar arrays mounted on panels (higher efficiency and areal mass); the pure SEP spacecraft does not employ a gimbal system, as it is assumed that attitude maneuvers can be used to steer the thrust vector; lastly, margins are taken into account.

Given the initial mass of the spacecraft in the pole-sitter orbit (as found in Table 2 for a given mission scenario), the optimal 1-year trajectory is used to compute the propellant mass m_{prop} needed for a given lifetime, $t_{mission}$. Despite the same trajectory is flown year after year, the controls are re-optimized locally, step by step, such that the SEP thrust is minimized point wise, and hence the propellant consumption is minimum, on that trajectory. Once the propellant mass is found, equations in Table 3 can be used to compute the payload mass m_{pl}. This is plotted, as a function of the lifetime, in Figure 7. Each plot refers to one spacecraft architecture (pure SEP, hybrid).

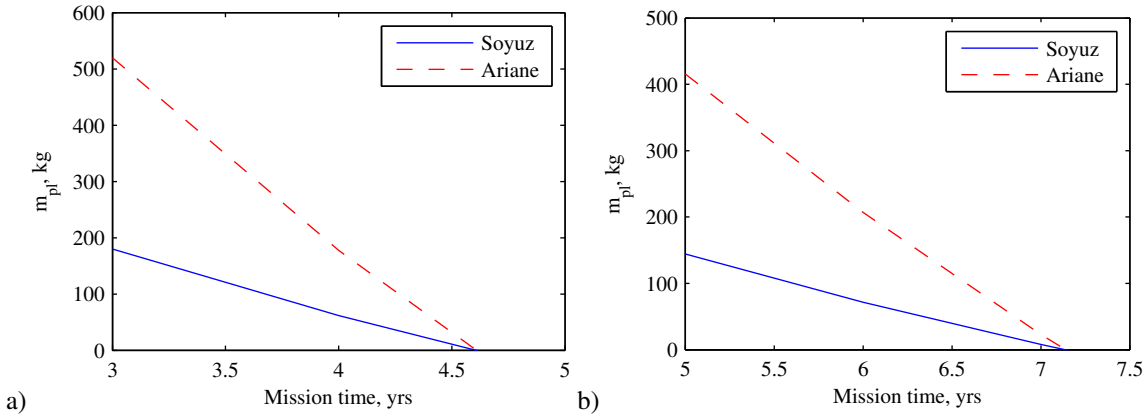

Figure 7. Payload mass (m_{pl}) as function of the mission lifetime, for the pure SEP spacecraft (a) and the hybrid spacecraft (b).

First, the mission lifetime does not depend on the injected total mass m_0, but only on the technology that is used to build the spacecraft. The lifetime for the pure SEP system is limited to about 4.5 years, while this value extends to about 7 years for the hybrid architecture. This result itself should be sufficient to justify the interest in the hybrid propulsion technology for this kind of mission, and in general for all those missions which require a continuous acceleration throughout the mission [20]. Furthermore, for the same injection mass m_0, the hybrid spacecraft can carry the same payload mass for a longer mission lifetime. Finally, fixing the spacecraft architecture, the payload mass scales with the injection mass.

We now wish to investigate possible payloads that could be used on the pole-sitter spacecraft. As noted in the introduction, the pole-sitter spacecraft could serve as a platform for Earth observation and science, and as a data relay for telecommunications. Concerning the former, taken into account the considerable distance of the spacecraft from the Earth, high-resolution imaging is limited to the near-visible part of the spectrum (from infrared to ultra-violet). As the resolution degrades with increasing wavelength, it is unlikely that sensing in the microwave band could provide some useful information. However, radio science can detect the total amount of radiation reflected and emitted by the Earth at the poles.

Candidate instruments for this kind of observations were found in the literature of deep space missions.[§§] In fact, their optics have long focal lengths and narrow field of views (FOVs), and they are therefore ideal for the pole-sitter. In particular, the NASA mission Galileo, launched in 1989 towards Jupiter and its satellites, was designed to perform observations of Jupiter's atmospheric composition, weather phenomena and auroras. Its Solid State Imaging (SSI) was a 800x800 CCD, 0.46 deg field of view telescope in the near visible range. Its aperture was 30 cm and weighed 29.7 kg. This instrument could resolve at about 27 km/pixel at the maximum predicted distance of the pole-sitter (2.74 million km). Galileo was also equipped with a Near-Infrared Mapping Spectrometer (NIMS), which could achieve a resolution of about 137 km on the pole-sitter, an Ultraviolet spectrometer (UVS) and a radiometer

[§§] Data extracted from the official websites of the programs managing agencies. Some data provided by Alex Coletti of SMRC.

(PPR). The mass of these three instruments combined was less than 40 kg. Despite the fact that the instruments used on this spacecraft are now outdated, they provide an idea of the data, resolution of imaging and mass of the payload.

The NASA Deep Space Climate Observatory (DSCOVR) was designed for Earth observation and science from the L_1 Lagrangian point, which lays at about 1.5 million km from the Earth, the same order of distance as the pole-sitter (where angular size of the Earth disc is about 0.5 deg). Despite that this mission was canceled during its design stage due to budget constraints, its payload would have been extremely similar to what could be used in a pole-sitter. DSCOVR's main payload is the Earth Polychromatic Imaging Spectrometer (EPIC), a 35 cm aperture near-visible telescope, which can be used to study ozone, aerosols, cloud fraction, thickness, optical depth, and height, sulfur dioxide, precipitable water vapor, volcanic ash, and UV irradiance. The instrument has a pixel matrix of 2048x2048 and a field of view of 0.62 deg, for a potential resolution on the pole-sitter of about 14 km/pixel. The mass of this instrument was predicted to be 39 kg.

The masses of each payload of the Galileo and DSCOVR missions never exceed 50 kg, therefore based on Figure 7, they are all suitable for both hybrid and SEP configurations missions, for lifetimes of about 4 years or more.

Note also that the power needed by any of these instruments is about two orders of magnitude lower than the power required by the SEP system, and therefore should not constitute a strong constraint on the power budget.

The pole-sitter spacecraft can also be used for uninterrupted data relay with the polar regions of the Earth, for example for telemedicine or medium-bandwidth real time scientific data transmission. In this case, the telecommunication subsystem would be the main payload of the spacecraft. However, even for planetary science, there will be a need to download a relatively large volume of data from the spacecraft to the Earth in a relatively short time (real-time high resolution imaging, for example). Considering the distance of the pole-sitter from the Earth, it is likely that a high-gain steerable antenna will be used for either or both of these tasks. High-gain Intelsat V – a telecommunication satellite – antennas weighed 30, 15 and 6 kg respectively. SUPERBIRD high-gain antenna had a mass of 47.1 kg. Considering that the data rate required for the pole-sitter mission would certainly be lower than that required by telecommunication spacecraft, we can estimate that the upper mass limit for this device would be 50 kg (assuming the RF telecommunication subsystem is part of the platform mass).

Certainly, an accurate determination of the mass of the telecommunication subsystem and the observation payload would require the definition of precise mission objectives, temporal and spatial resolution of the images, and an estimation of the required data-rate. However, for a preliminary definition of spacecraft design points, we consider a mass of 100 kg for both observation and telecommunication payloads. With this payload mass value, the design points for the four scenarios are described in Table 4. They represent the condition in which all the capacity of the launcher is used for the pole-sitter spacecraft; however, it is possible to downscale any of the four scenarios (at the cost of a reduction of mission lifetime).

Launching the spacecraft with Soyuz, the lifetime is 3.6 years if the spacecraft is using pure SEP technology, or 5.6 years if using hybrid propulsion. These lifetimes extend to 4.24 and 6.58 years when launching with Ariane 5 for the two architectures respectively. The subsystem design also allows computing the mass of the other subsystems, some of them are reported in the same table. The size of the total sail assembly (reflective surface and thin film solar cells) of the hybrid spacecraft, assuming a square assembly, is 191 m for the Soyuz launch, and 324 m for the Ariane 5

launch. The hybrid configuration furthermore allows having a lower power budget, by reducing the thrust needed per unit mass of the spacecraft from the SEP thruster. For the pure SEP spacecraft, the maximum power required by the SEP system is 6 kW (Soyuz) and 17.4 kW (Ariane 5). For the hybrid case, instead, the power is 5.2 kW (Soyuz) and 15 kW (Ariane), despite the fact that the total injected mass of the spacecraft, m_0, is slightly larger than in the SEP case.

Table 4. Design points. Masses are without margins.

Architecture	Pure SEP		Hybrid	
Launcher	Soyuz	Ariane 5	Soyuz	Ariane 5
Lifetime, $t_{mission}$, yrs	3.6	4.24	5.6	6.58
Payload mass, m_{pl}, kg	100	100	100	100
Pole-sitter injection mass, m_0, kg	1537	4439	1595	4599
SEP mass, $n_{thrusters} m_{thruster}$, kg	121	348	104	299
Propellant mass, m_{prop}, kg	675	2192	698	2242
Other subsystems mass, m_{other}, kg	259	674	269	707
Solar array/TFSC area, A_{SA} / A_{TF}, m^2	44	127	121	349
Solar sail mass (reflective), m_s, kg	-	-	182	524
Total sail area (reflective + TFSC), A, m^2	-	-	191 × 191	324 × 324
Maximum SEP thrust, T_{max}, mN	269	776	231	667
Maximum SEP power, $P_{SEP,max}$, kW	6	17.4	5.2	15.0

7. Transfers between north and south

Due to the tilt of the Earth's rotational axis with respect to the ecliptic plane, the north and south poles are alternately situated in darkness for 6 months per year. For observations performed in the visible part of the spectrum, this significantly constrains the mission scientific return. Therefore, an additional transfer is introduced that allows the pole-sitter spacecraft to change between pole-sitter orbits above the north and south poles before the start of the Arctic and Antarctic winters, see Figure 3. For that, the SEP and hybrid pole-sitter orbits shown in Figure 4 are mirrored in the ecliptic plane.

Viewed in the synodic frame, the poles are illuminated when the spacecraft is in the Sun-ward part of the pole-sitter orbit, see Figure 8. Ideally, this means that the pole-sitter spacecraft would follow the north pole-sitter orbit from March to September and the south pole-sitter orbit from September to March. Clearly in reality this is not feasible since some time needs to be allowed for the spacecraft to transfer from north to south and vice-versa.

The concept of transfers between north and south pole-sitter orbits has been introduced before [22], and is applied in this section to the optimal SEP and hybrid pole-sitter orbits of Figure 4 (using the respective types of propulsion to

perform the transfer). Also, for both propulsion strategies, both the Soyuz and Ariane 5 launch cases will be considered together with the corresponding values for the maximum thrust magnitude as provided in Table 2.

The work in Reference [22] showed that two types of transfers can be considered: a short transfer that takes less than half a year and a long transfer that takes between half a year and one year. In order to maximize the observation time during the mission, this work will only consider the short transfer, which means that the departure and arrival windows for a north-to-south transfer are as indicated in Figure 8. Departure thus takes place between summer and autumn (June – September), while arrival takes place between autumn and winter (September – December), where this paper conventionally refers to the seasons in the northern hemisphere.

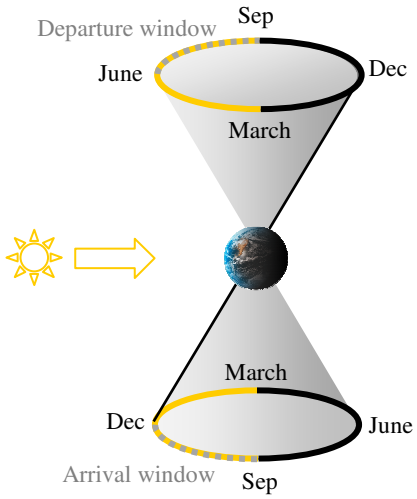

Figure 8. Schematic of dark (black line) and light (yellow line) conditions on the north and south poles during the year and departure and arrival windows (dotted) for a north-to-south transfer.

Due to the symmetry of the problem, the optimal transfers from north to south can also be used to transfer from south to north. For that, it is assumed that the lower mass at the start of the south to north transfer (or any subsequent transfer) does not influence the trajectory to great extent.

The transfers between north and south pole-sitter orbits are optimized to minimize the SEP propellant required to perform the transfer. Since previous research [22] showed that these minimum propellant transfers lead to rather long transfer times (and thus to rather short periods in which observation can take place), additional optimizations are carried out that minimize a sum of the propellant consumption and the time of flight through the use of a weight factor, w. This results into the following objective function:

$$J = \frac{m_{t,0} - m_{t,f}}{m_{t,0}} + w\frac{t_{t,f} - t_{t,0}}{2\pi} \tag{7}$$

with the subscripts '$t,0$' and 't,f' indicating the start and end of the transfer. Clearly, for $w = 0$ the minimum propellant case is considered.

The optimal control problem is once again solved with PSOPT. End-point constraints are included to ensure that the initial and final conditions coincide with the north and south pole-sitter orbits in the departure and arrival windows indicated in Figure 8, including the mass at the start of the transfer. This mass is computed by considering that the

north-to-south transfer takes place in the first year of the mission and after injection of the masses provided in Table 2 at winter solstice.

Initial guesses for the pure SEP, minimum propellant transfer are created using a shape based approach where a particular shape of the transfer (that satisfies the end-point constraints) is assumed and the controls required to follow that particular shape are extracted from the equations of motion. The optimal SEP transfer is subsequently used as an initial guess for non-zero values for the weight factor and also to generate the minimum propellant, hybrid transfers.

7.1 Results

The results for the pure SEP case are shown in Figure 9 and Figure 10, where the following values for the weight factor are used: $w = \begin{bmatrix} 0 & 0.25 & 0.5 & 1.0 & 1.5 \end{bmatrix}$. Figure 9 clearly shows a resemblance between the Soyuz and Ariane 5 cases, once again indicating the scalability of the transfer with the mass. As indicated before, this is a result of the fact that the maximum SEP thrust magnitude scales proportionally with the increase in the injected mass that the Ariane 5 launch can establish, see Table 2. Any remaining differences between the Soyuz and Ariane 5 solutions (e.g. in the acceleration profile for $w = 0$ in Figure 9c) can be attributed to a premature convergence of PSOPT.

Figure 10a furthermore shows the gain in observation time per pole that can be achieved by increasing the weight factor. For the values considered here, observation times of up to 94 days can be achieved. This comes, however, at the cost of an increase in the propellant consumption. This also becomes clear from Figure 9d which also includes the propellant consumption in the pole-sitter orbit itself and can therefore provide insights into how demanding the north-to-south pole-sitter transfers are. It becomes clear that, depending on the value for the weight, the transfer can provide a saving in propellant consumption, which can be used to significantly extend the mission lifetime of the pure SEP mission. This is shown in Figure 10b, which provides the mass profile throughout the pole-sitter mission (Soyuz launch) when the north-to-south transfers are taken into account and when they are not. The figure clearly shows the gain in propellant consumption that the transfers can establish. For example, for $w = 0$ the gain is 279.6 kg after 5 years. Increasing the weight factor leads to smaller gains and for $w = 1.5$ even a small loss of 45.3 kg can be observed after 5 years.

Because very similar results can be obtained for the hybrid case, detailed plots are omitted here. However, summarized results are provided in Figure 10a, which shows that the hybrid case can obtain similar observation times as for the pure SEP case, but for much lower propellant consumption.

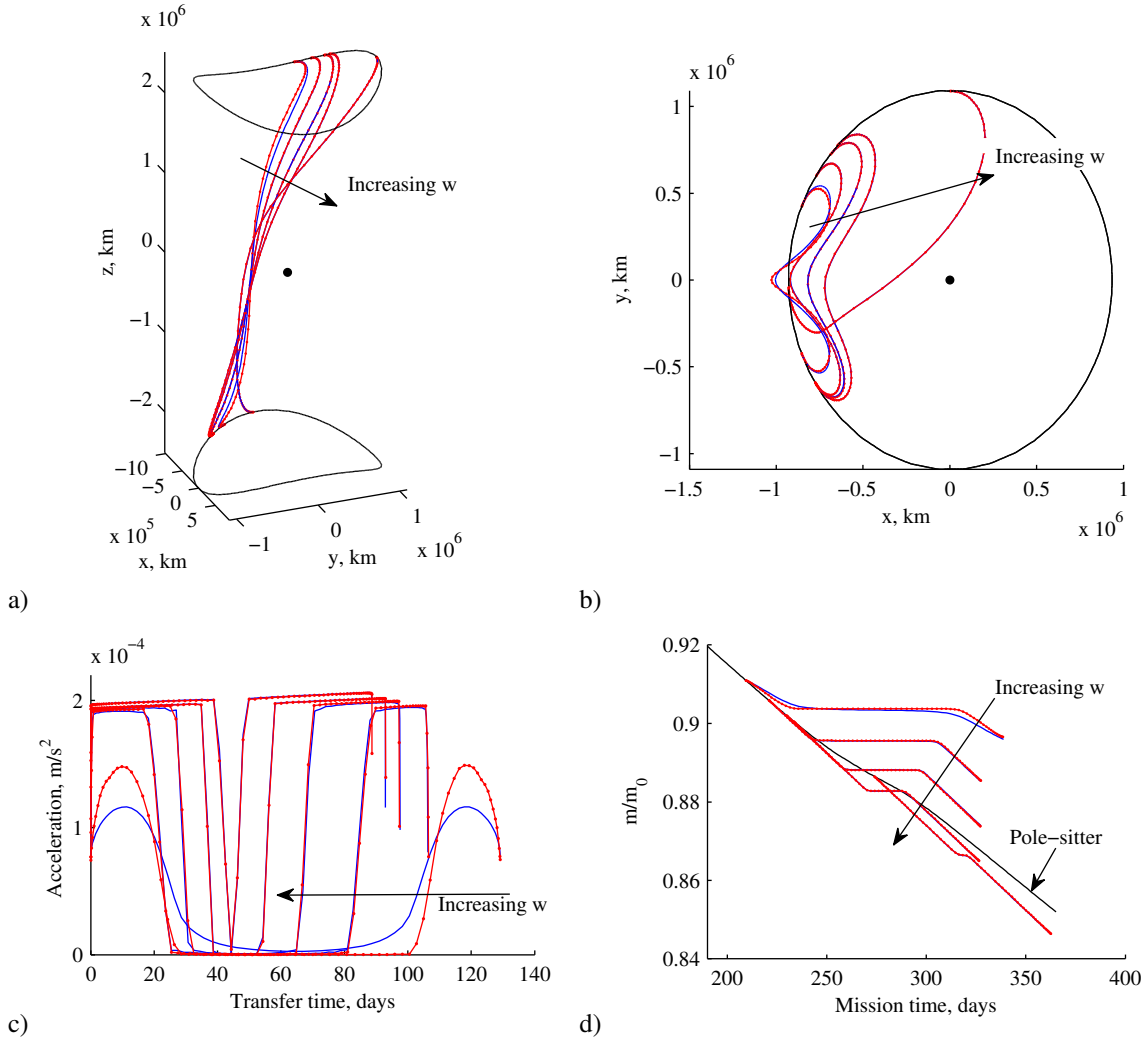

Figure 9. Optimized, pure SEP north-to-south pole-sitter transfers for different values of the objective weight factor, *w* = [0 0.25 0.5 1.0 1.5], and for a Soyuz launch (solid lines) and Ariane 5 launch (dotted lines). a-b) Transfers in the synodic reference frame. c) Acceleration as a function of the time in the transfer. d) Ratio of current mass and mass at injection as a function of the mission time.

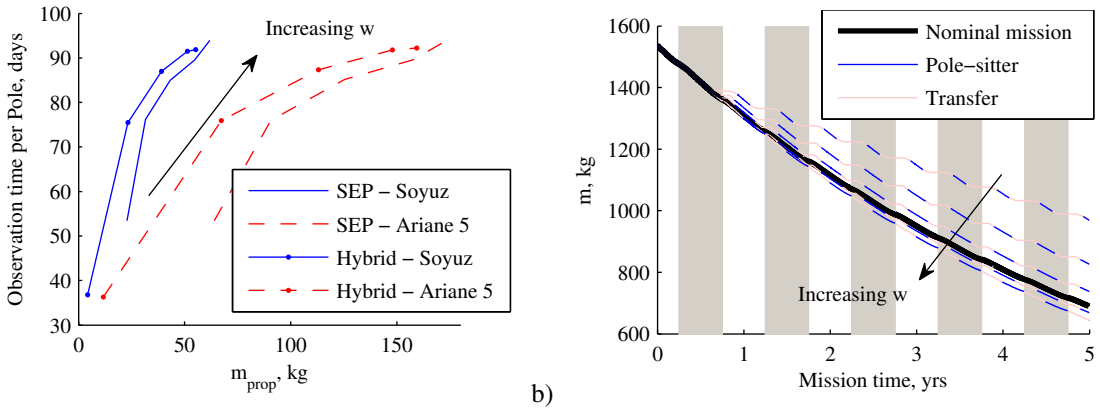

Figure 10. a) Observation time as a function of the propellant consumption for the SEP and hybrid cases. b) Mass profile throughout the SEP pole-sitter mission (Soyuz launch) including the north-to-south pole-sitter transfer. Shaded areas highlight the half of the year when the north pole is lit.

Conclusions

In this paper a full, preliminary mission analysis and systems design of a near-term and far-term pole-sitter mission is provided, where the distinction comes from the use of either existing, solar electric propulsion (SEP) or more far-term hybrid SEP and solar sail propulsion. The platform would provide a vantage view point on either pole of the Earth, with potentially unlimited temporal resolution by means of one spacecraft only. Optimal transfers from north to south and vice-versa allow to observe the pole that is lit, at no extra cost in terms of propellant consumption. Moreover, in some particular cases propellant savings can be achieved through the use of these transfers, allowing for an extension of the mission lifetime or alternatively an increase in the payload mass.

The main concern regarding this mission is related to the considerable distance of the spacecraft from Earth. However, it is shown that instruments which flew on the Galileo mission and others that were designed for the DSCOVR Earth observation mission from L_1 would enable, on the pole-sitter, the study of the atmosphere, large-scale, rapidly-changing weather phenomena, auroras, sea ice changes, and other phenomena that require modest spatial resolution. It is also possible to employ a high-gain antenna for using the spacecraft as continuous data-relay with scientific stations in Antarctica and other high-latitude settlements. Using the full potential of either a Soyuz or Ariane 5 launch vehicle, a systems mass budget showed that it is potentially possible to carry these payloads for at least 4 years for the short-term SEP-only mission, and 6 years or more for the far-term hybrid mission.

Acknowledgements

This work was funded by the European Research Council, as part of project 227571 VISIONSPACE. The authors thank Dr. Victor M. Becerra, of the School of Systems Engineering, University of Reading, Reading, UK for providing the software PSOPT freely, as well as advices on its use. Many thanks also to Alex Coletti, of SMRC, for valuable discussions on instruments for polar observation and for providing some of the data presented in this paper.

References

[1] M. Ceriotti, C.R. McInnes, B.L. Diedrich, The pole-sitter mission concept: an overview of recent developments and possible future applications, in: 62nd International Astronautical Congress (IAC2011), Cape Town, South Africa, 2011.
[2] P.C. Anderson, M. Macdonald, Extension of Earth orbits using low-thrust propulsion, in: 61st International Astronautical Congress (IAC 2010), Prague, Czech Republic, 2010.
[3] P.C. Anderson, M. Macdonald, Extension of the Molniya orbit using low-thrust propulsion, in: 21st AAS/AIAA Space Flight Mechanics Meeting, AIAA, New Orleans, USA, 2011.
[4] C.R. McInnes, P. Mulligan, Final report: telecommunications and Earth observations applications for polar stationary solar sails, in, National Oceanographic and Atmospheric Administration (NOAA)/University of Glasgow, Department of Aerospace Engineering, 2003.
[5] J.M. Driver, Analysis of an arctic polesitter, Journal of Spacecraft and Rockets, 17 (1980) 263-269.
[6] C.R. McInnes, Solar Sailing: Technology, Dynamics and Mission Applications, Springer-Praxis Books in Astronautical Engineering, Springer-Verlag, Berlin, 1999.
[7] F.A. Tsander, From a scientific heritage (Translation of "Iz nauchnogo naslediya"), in: NASA Technical Translation, NASA, 1969.
[8] O. Mori, H. Sawada, R. Funase, T. Endo, M. Morimoto, T. Yamamoto, Y. Tsuda, Y. Kawakatsu, J.i. Kawaguchi, Development of first solar power sail demonstrator - IKAROS, in: 21st International Symposium on Space Flight Dynamics (ISSFD 2009), CNES, Toulouse, France, 2009.
[9] H. Baoyin, C.R. McInnes, Solar sail equilibria in the elliptical restricted three-body problem, Journal of Guidance, Control, and Dynamics, 29 (2006) 538-543.
[10] G. Mengali, A.A. Quarta, Solar sail trajectories with piecewise-constant steering laws, Aerospace Science and Technology, 13 (2009) 431-441.
[11] R.L. Forward, Statite: a spacecraft that does not orbit, Journal of Spacecraft and Rockets, 28 (1991) 606-611.
[12] T.J. Waters, C.R. McInnes, Periodic orbits above the ecliptic in the solar-sail restricted three-body problem, Journal of Guidance, Control, and Dynamics, 30 (2007) 687-693.
[13] M. Ceriotti, C.R. McInnes, Generation of optimal trajectories for Earth hybrid pole-sitters, Journal of Guidance, Control, and Dynamics, 34 (2011) 847-859.
[14] M. Leipold, M. Götz, Hybrid photonic/electric propulsion, in, Kayser-Threde GmbH, Munich, Germany, 2002.
[15] S. Baig, C.R. McInnes, Artificial three-body equilibria for hybrid low-thrust propulsion, Journal of Guidance, Control, and Dynamics, 31 (2008) 1644-1655.
[16] G. Mengali, A.A. Quarta, Tradeoff performance of hybrid low-thrust propulsion system, Journal of Spacecraft and Rockets, 44 (2007) 1263-1270.
[17] J. Simo, C.R. McInnes, Displaced periodic orbits with low-thrust propulsion, in: 19th AAS/AIAA Space Flight Mechanics Meeting, American Astronautical Society, Savannah, Georgia, USA, 2009.
[18] J. Heiligers, M. Ceriotti, C.R. McInnes, J.D. Biggs, Displaced Geostationary Orbit Design Using Hybrid Sail Propulsion, Journal of Guidance, Control, and Dynamics, 34 (2011) 1852-1866.
[19] M.A. Lazzara, A. Coletti, B.L. Diedrich, The possibilities of polar meteorology, environmental remote sensing, communications and space weather applications from Artificial Lagrange Orbit, Advances in Space Research, 48 (2011).
[20] M. Ceriotti, C.R. McInnes, Systems design of a hybrid sail pole-sitter, Advances in Space Research, 48 (2011) 1754–1762.
[21] J. Heiligers, M. Ceriotti, C.R. McInnes, J.D. Biggs, Design of optimal Earth pole-sitter transfers using low-thrust propulsion, in: 62nd International Astronautical Congress (IAC2011), Cape Town, South Africa, 2011.
[22] J. Heiligers, M. Ceriotti, C.R. McInnes, J.D. Biggs, Design of optimal transfers between North and South pole-sitter orbits, in: 22nd AAS/AIAA Space Flight Mechanics Meeting, Charleston, South Carolina, USA, 2012.
[23] M.H. Kaplan, Modern spacecraft dynamics and control, John Wiley and Sons, Inc., New York, 1976.
[24] J. Brophy, Advanced ion propulsion systems for affordable deep-space missions, Acta Astronautica, 52 (2003) 309-316.
[25] H.J. Leiter, R. Killinger, H. Bassner, J. Müller, R. Kukies, T. Fröhlich, Development and performance of the advanced radio frequency ion thruster RIT-XT, in: 28th International Electric Propulsion Conference (IEPC 2003), Toulouse, France, 2003.
[26] S. Marcuccio, L. Paita, M. Saviozzi, M. Andrenucci, Flight demonstration of FEEP on get away special, in: 33rd AIAA/ASME/SAE/ASEE Joint Propulsion Conference and Exhibit, AIAA, Cleveland, OH, USA, 1998.
[27] R. Funase, O. Mori, Y. Tsuda, Y. Shirasawa, T. Saiki, Y. Mimasu, J. Kawaguchi, Attitude control of IKAROS solar sail spacecraft and its flight results, in: 61st International Astronautical Congress (IAC 2010), IAF, Prague, Czech Republic, 2010.
[28] B. Dachwald, G. Mengali, A.A. Quarta, M. Macdonald, Parametric model and optimal control of solar sails with optical degradation, Journal of Guidance, Control, and Dynamics, 29 (2006) 1170-1178.
[29] J.i. Kawaguchi, Y. Mimasu, O. Mori, R. Funase, T. Yamamoto, Y. Tsuda, IKAROS - Ready for lift-off as the world's first solar sail demonstration in interplanetary space, in: 60th International Astronautical Congress (IAC 2009), International Astronautical Federation, Daejeon, Korea, 2009.
[30] L. Johnson, M. Whorton, A. Heaton, R. Pinson, G. Laue, C. Adams, NanoSail-D: A solar sail demonstration mission, Acta Astronautica, 68 (2011).
[31] D.M. Murphy, T.W. Murphey, P.A. Gierow, Scalable solar-sail subsystem design concept, Journal of Spacecraft and Rockets, 40 (2003) 539-547.

[32] V.M. Becerra, PSOPT optimal control solver user manual, in, 2009.
[33] V.M. Becerra, Solving complex optimal control problems at no cost with PSOPT, in: IEEE Multi-conference on Systems and Control, IEEE, Yokohama, Japan, 2010, pp. 1391-1396.
[34] A. Wächter, L.T. Biegler, On the implementation of a primal-dual interior point filter line search algorithm for large-scale nonlinear programming, Mathematical Programming, 106 (2006) 25-57.
[35] T.S.C. Starsem, Soyuz User's Manual (ST-GTD-SUM-01 - issue 3 - revision 0), in, 2001.
[36] D.A. Vallado, Fundamentals of Astrodynamics and Applications, 3rd Edition ed., Space Technology Library, New York, USA, 2007.
[37] Arianespace, Ariane 5 User's Manual - Issue 5 - Revision 0, in, 2008.
[38] J.R. Wertz, W.J. Larson, Space mission analysis and design, third edition, in: Space technology library, Microcosm press/Kluwer Academic Publishers, El Segundo, California, USA, 1999.
[39] S. Kitamura, Y. Ohkawa, Y. Hayakawa, H. Yoshida, K. Miyazaki, Overview and research status of the JAXA 150-mN ion engine, Acta Astronautica, 61 (2007) 360-366.
[40] R. Gershman, C. Seybold, Propulsion trades for space science missions, Acta Astronautica, 45 (1999) 541-548.

Biographies

Jeannette Heiligers

Jeannette Heiligers is a Ph.D. candidate at the Advanced Space Concepts Laboratory at the University of Strathclyde. She obtained her M.Sc. cum laude in Aerospace Engineering from Delft University of Technology, the Netherlands. During her Master she participated in the mission analysis for the European Student Moon Orbiter mission of the European Space Agency at the Department of Aerospace Engineering of the University of Glasgow and her thesis covered the multi-objective optimization of both high- and low-thrust trajectories for an asteroid sample return mission. Funded by the European Research Council, the PhD currently focuses on the orbital dynamics of non-Keplerian orbits using hybrid solar sail and solar electric propulsion and the optimization of transfers to and between non-Keplerian orbits.

Matteo Ceriotti

Dr. Matteo Ceriotti received his M.Sc. summa cum laude from Politecnico di Milano (Italy) in 2006 with a thesis on planning and scheduling for planetary exploration. In 2010, he received his Ph.D. on “Global Optimisation of Multiple Gravity Assist Trajectories” from the Department of Aerospace Engineering of the University of Glasgow (United Kingdom). During 2009-2012, Matteo was a research fellow at the Advanced Space Concepts Laboratory, University of Strathclyde, Glasgow, leading the research theme “Orbital Dynamics of Large Gossamer Spacecraft” in the ERC project VISIONSPACE. In 2012, he returned to the University of Glasgow as a lecturer in Space Systems Engineering, within the School of Engineering, division of Systems, Power and Energy. He is AIAA member.

Colin McInnes

Colin McInnes is Director of the Advanced Space Concepts Laboratory at the University of Strathclyde. His work spans highly non-Keplerian orbits, orbital dynamics and mission applications for solar sails, spacecraft control using artificial potential field methods and is reported in over 100 journal papers. Recent work is exploring new approaches to spacecraft orbital dynamics at extremes of spacecraft length-scale to underpin future space-derived products and services. McInnes has been the recipient of awards including the Royal Aeronautical Society Pardoe Space Award (2000), the Ackroyd Stuart Propulsion Prize (2003) and a Leonov medal by the International Association of Space Explorers (2007).

James Biggs

James Biggs received the B.Sc. degree in Mathematics from the University of Sussex, Brighton, UK in 1998, the M.Sc. degree in Nonlinear Dynamics and Chaos from University College London, London, U.K. in 1999 and the PhD degree from the University of Reading, U.K. He is currently an associate director of the Advanced Space Concepts Laboratory and lecturer at the University of Strathclyde, Glasgow. Presently his research interests are focused on using dynamical systems theory, control theory and differential geometry to design novel spacecraft orbits as well as optimal attitude maneuvers.